First-principles calculation of x-ray absorption spectra and x-ray magnetic circular dichroism of ultrathin Fe films on $BaTiO_3$(001)

St. Borek, I. Maznichenko, G. Fischer, W. Hergert, and I. Mertig
Institut für Physik, Martin-Luther-Universität Halle–Wittenberg, D-06099 Halle, Germany

A. Ernst and S. Ostanin
Max-Planck-Institut für Mikrostrukturphysik, Weinberg 2, D-06120 Halle, Germany

A. Chassé
Institut für Physik, Martin-Luther-Universität Halle–Wittenberg, D-06099 Halle, Germany

(Received 20 July 2011; revised manuscript received 13 February 2012; published 19 April 2012)

First-principles calculations of x-ray absorption spectra (XAS) and the related x-ray magnetic circular dichroism (XMCD) are presented for ultrathin Fe layers on a $BaTiO_3$ (BTO) single-crystal surface within the framework of density functional theory. We have investigated the dependence of XAS and XMCD of Fe $L_{2,3}$ edges as a function of Fe layer thickness (1–3 ML) and on polarization direction of BTO. The calculations give a detailed insight concerning the relation between structural, electronic, and magnetic properties at the multiferroic interface Fe/BTO. In dependence on the Fe layer thickness we find characteristic features in the related XMCD, which depend strongly on the interface structure. The critical temperature of the ultrathin Fe layer is calculated to be between 170 to 230 K.

DOI: 10.1103/PhysRevB.85.134432 PACS number(s): 71.15.Mb, 11.80.La, 71.20.−b, 77.84.Cg

I. INTRODUCTIONlabelintro

The system Fe/BTO is a prototype of a multiferroic interface showing magnetoelectric coupling. Recently, first-principles calculations of Fe/BTO multilayers[1–3] predicted the dependence on the magnetic properties on the polarization direction of BTO. The magnetoelectric effect, driven by the Fe/BTO interface bonding, results in changing the magnetic moments of Fe and Ti atoms.[1] The induced magnetic moments of Ti and O atoms at the interface depend strongly on the thickness of the Fe layers.[2] Besides, a change of the long-range magnetic order of the Fe layer was found as a function of thickness: the ferromagnetic phase of 1 ML Fe/BTO changed into a ferrimagnetic phase in the 2 ML case and returned into a ferromagnetic order of 3 ML Fe.[3] Layer-resolved induced magnetic moments of Fe near the Fe/BTO interface were discussed in the framework of tricomponent superlattices,[4] where the induced magnetization results from screening charges.

Recently, induced magnetic moments of Ti and O atoms were experimentally verified in the multiferroic systems Fe/BTO/LSMO and Co/BTO/LSMO.[5] In the spectroscopic measurements of x-ray absorption and x-ray resonant magnetic scattering the Ti $L_{2,3}$ and the O K edges were considered. In all experiments the Fe (Co) layer thickness was fixed at 2 nm (1.2 nm). Consequently, the x-ray absorption spectra of the Fe $L_{2,3}$ edge and the x-ray magnetic circular dichroism show typical bulk Fe (Co) features.

The theoretical investigations[1–4] are performed in the limit of ultrathin Fe layers to study the thickness dependence of x-ray absorption and x-ray magnetic dichroism and to gain insight into the origin of magnetoelectric coupling. Experimental verification is still missing in this limit.

X-ray absorption spectra (XAS) and x-ray magnetic dichroism (XMCD) are state-of-the-art methods to determine both the electronic and magnetic structure of materials including site and valence band information as well as element-specific structure and magnetization. In addition to the chemical selectivity of XAS, XMCD gives information on the magnetic spin and orbital moments of the excited atoms.

XMCD originates from coupling between the photon spin and the atomic magnetic moments, which gives rise to a difference between the absorption cross sections measured with the magnetic field parallel or antiparallel to the photon wave vector. XMCD was observed by Schütz *et al.*[6] at the Fe K edge. In the soft x-ray range it was measured on the Ni $L_{2,3}$ edges by Chen *et al.*[7] Both, experiment and theory of XMCD are well documented. Within this paper we give only a short summary concerning the study of the XMCD of thin Fe layers and related interface properties.

XAS and XMCD have been applied with great success in the investigation of magnetic properties of thin Fe layers on different metallic substrates such as Cu, Ag, Au and Rh, Pd, and Pt (see Refs. 8,9 and references therein). Besides fundamental research of magnetism in low dimensions, studies were motivated by the search of induced magnetic moments at the interface.[10] Hybridization and exchange interaction caused enhanced magnetic spin and orbital moments in ultrathin Fe layers.[11] Recently a magnetic model of the archetype system fcc-Fe/Cu(001) was introduced, where, in combination with first-principles calculations, magnetic noncollinearity was directly demonstrated.[12] The electronic and magnetic coupling between Fe and oxides is determined by the complex interface resulting from oxide reduction and metal oxidation, which were investigated in the study of magnetic tunnel junctions such as the Fe/MgO/Fe(001) system.[13,14] It has been found that the growth of Fe layers depends strongly on the preparation methods.[15] The interplay between magnetic properties and morphology was detected for thin iron films deposited on MgO/Ag(001) substrates. The onset of ferromagnetism above 4.5 ML at room temperature could be ascribed to the transition

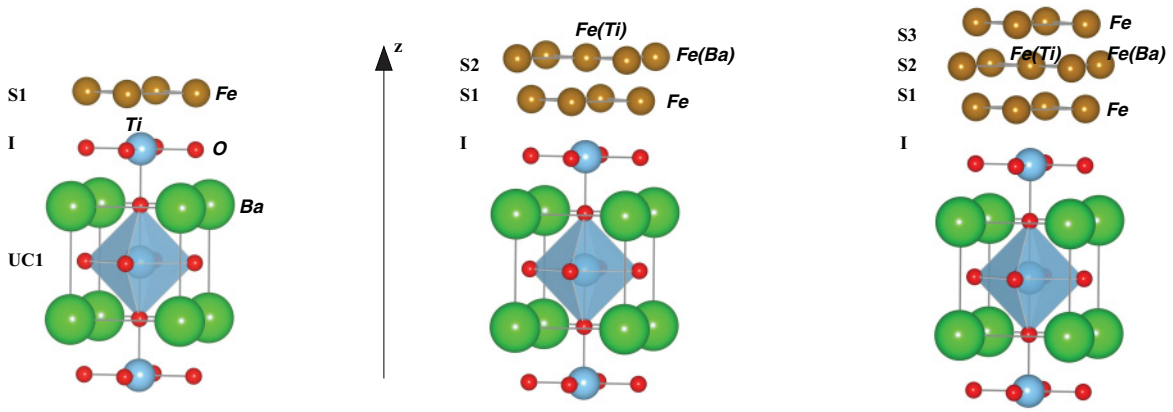

FIG. 1. (Color online) Construction of the supercells for 1 ML, 2 ML, and 3 ML Fe/BTO(001).[25]

from a three-dimensional to a two-dimensional growth mode of the iron deposit.[16]

Fe layers on NiO and CoO single crystal surfaces are often considered as prototype systems of FM-AFM interfaces. Strong evidence for an interfacial region (1–3 atomic layers) was found, where NiO was reduced and the Fe overlayer was oxidized in the Fe/NiO/Ag(001) system.[17] The reduced magnetic moments in Fe films on NiO(001) crystals were explained by paramagnetic FeO formed at the interface in the growth process.[18]

The Fe/BTO interface has been investigated experimentally by different methods. Until now the preparation of ultrathin Fe films on BTO single crystals or BTO thin films bears a challenge for experimental verification. Pioneering work has been done by Brivio *et al.*[19,20] High-quality 1–3 nm Fe films were epitaxially grown on BTO/STO(001).[20] Sahoo *et al.*[21] and Yu *et al.*[22] prepared polycrystalline films on BTO(001) and BTO/STO(001) of 10-nm and 30-nm thickness, respectively. Garcia *et al.*[23] used 5-nm thick Fe films for Fe/BTO tunnel barriers. In the multiferroic system investigated by Valencia *et al.*[5] (2-nm thick Fe) the Fe layer consists of textured crystallites. Both x-ray absorption spectra and the related magnetic dichroism were typical of bulk bcc Fe. This result was found also by Garcia *et al.*[23]

Until now we have no experimental information about the Fe/BTO interface concerning the dependence of the magnetoelectric effect and related phenomena on the Fe layer thickness. The focus of this paper is to get the resolution of layer-dependent effects in spectroscopic methods such as x-ray absorption spectroscopy and the related magnetic dichroism. Therefore, we present first-principles calculations of x-ray absorption spectra of ultrathin Fe films (1–3 ML) on BTO(001). The aim of this theoretical study is to obtain the XMCD of Fe $L_{2,3}$ edges as a function of Fe layer thickness and polarization direction of BTO.

A fully relativistic Green's function method is applied to investigate the spectroscopic properties of the system. We take the relaxed atomic positions calculated by means of a pseudopotential formalism[2,3] as starting point of our studies. Scalar-relativistic calculations are used to compare the magnetic spin moments with the recently published values. We extend these to fully relativistic calculations (which are the basis of our XMCD computations), whereby we obtain the magnetic orbital moments as well. The long-range magnetic order of the system is investigated within a Heisenberg model.

The organization of the paper is as follows: We briefly introduce in Sec. II our multicode approach. At first we present in Sec. III calculated distances, magnetic spin, and orbital moments. The second part shows our theoretical results of x-ray absorption spectra and related XMCD. The last part is dedicated to the investigations concerning the critical temperature of this system. We conclude with a short summary and outlook in Sec. IV.

II. MULTICODE APPROACH

We use a multicode approach to calculate the structural, electronic, and magnetic properties of the Fe/BTO(001) system in dependence on both Fe layer thickness and direction of the electric polarization **P** of BTO(001) with respect to the surface.

Supercells are constructed to model the Fe/BTO system. The supercells, as shown in Fig. 1, consist of five unit cells (UCs) of BTO (originally with $P4$ mm symmetry) with a TiO_2-terminated (001) surface (interface I), Fe layers ($S1$, $S2$, $S3$), and five layers of empty spheres (not shown) to simulate the vacuum. The TiO_2 termination of BTO was confirmed recently in an experimental and theoretical study of ultrathin BTO films grown on Fe(001).[24]

The polarization **P** in the ferroelectric BTO arises by shifting Ti and O atoms along the z axis in opposite directions, which leads to a tetragonal distortion of the unit cell. The [100] direction of Fe(bcc) is aligned along the [110] direction of BTO(001). In the first Fe layer ($S1$) the Fe atoms ($Fe_{1,2}$) are placed on top of O atoms of the TiO_2-terminated BTO(001) surface. In the second layer ($S2$) Fe atoms are at two different positions: on top of Ti (Fe_{Ti}) and Ba (Fe_{Ba}) with respect to the TiO_2 interface. In the third layer $S3$ again Fe atoms ($Fe_{3,4}$) are on top of Fe atoms of the first Fe layer $S1$ like in a distorted bcc structure. Note, that there are two Fe atoms per unit cell in each Fe layer.

The structural relaxation of the systems is performed by the Vienna *Ab initio* Simulation Package (VASP).[26,27] The fully relaxed Fe/BTO supercell data are transfered to a spin-resolved fully relativistic Korringa-Kohn-Rostoker (SPR-KKR) code.[28–32]

TABLE I. Full relaxed structural distances in dependence on the Fe layer thickness and the direction of the electric polarization **P**. Ti* and O^* are the positions in the bulklike region of the BTO slab.

		1 ML Fe		2 ML Fe		3 ML Fe	
$d_\perp$ [Å]		P_{up}	P_{dn}	P_{up}	P_{dn}	P_{up}	P_{dn}
S3	Fe-Fe(Ba)					1.114	1.134
S2	Fe(Ba)-Fe			1.054	1.856	1.241	1.218
S2	Fe(Ti)-Ti			2.918	2.971	3.121	3.214
S1	Fe-O	1.781	1.774	1.855	1.856	1.849	1.843
I	Ti-O_{in} I	0.068	− 0.019	0.037	− 0.046	0.062	− 0.040
	Ti-O	2.058	1.940	1.988	1.905	2.036	1.951
	Ti*-O^*_{in}	0.086	− 0.086	0.086	− 0.086	0.086	− 0.086
	Ti*-O*	2.029	1.881	2.029	1.881	2.029	1.881

With the Green's function $G(E)$ of the system all quantities of interests can be calculated. In particular, we consider the density of states $n(E)$ and the magnetic moments (spin moment m_s, orbital moment m_o).[33] The x-ray absorption coefficient $\mu^\lambda(E)$ in dependence on energy E and polarization λ of x rays follows also in a straightforward way by means of Green's function method.[34]

The term magnetic dichroism characterizes the change of the x-ray absorption spectrum when the relative orientation of the helicity of circularly polarized light ($\lambda = \pm$) and the sample magnetization **M** is switched.[35] In our calculations the direction of **M** ($||\, z$ axis; Fig. 1) is fixed and the helicity of the incident light is changed from right (–) to left (+) circularly polarized light. The calculated x-ray absorption coefficient $\mu^\pm(E)$ and the difference for the Fe $L_{2,3}$ edges

$$\Delta\mu = \mu^- - \mu^+ \tag{1}$$

is normalized to the number of Fe atoms in the unit cell. All x-ray absorption spectra are calculated using the fully relativistic SPR-KKR code.[36]

The experimental proof of our spectroscopical predictions requires information about the critical temperatures of the Fe layers. Exchange constants J are extracted from the *ab initio* multiple-scattering calculations. Computations of the critical temperatures are performed by means of Monte Carlo simulations of the classical Heisenberg model.[37–39]

III. RESULTS AND DISCUSSION

A. Structure and magnetism

The starting point of all XAS and XMCD calculations is the relaxed structure of the supercells. In the applied VASP method based on projector-augmented wave (PAW) pseudopotentials[26,27] the plane-wave basis cutoff energy is 600 eV. After relaxation the calculated forces are less than 0.5×10^{-2}eV/Å. The Brillouin zone of the slab is sampled during the force minimization with a $10 \times 10 \times 6$ k-point Monkhorst-Pack mesh.[40] The in-plane lattice constant of BTO amounts 3.943 Å.

The relaxed structural parameters are summarized in Table I and agree with the previously published values of Fechner *et al.*[2,3] We emphasize attention to the reduced in-plane lattice constant (2.79 Å) and next-neighbor distance of Fe atoms in the multilayer system in comparison to the Fe-bcc bulk crystal ($a_0 = 2.87$ Å). At the interface I the relaxation of Ti and O atoms leads to reduced tetragonal distortions with respect to BTO bulk.

In Table II the local magnetic spin moments m_s are summarized obtained in the framework of our scalar-relativistic KKR calculations.[32] These calculations are indicated for a direct comparison of our results using atomic sphere approximation (ASA), which works without shape approximation to the crystal potential, with the recently published full-potential computations.[3] Our KKR-ASA results reflect all general trend of the magnetic properties in the considered system. The spin magnetic moments of Fe atoms are in good agreement with

TABLE II. Calculated magnetic spin moments m_s (scalar-relativistic KKR-ASA method) in dependence on the thickness of Fe layers and the direction of electric polarization **P** ($\mathbf{P}_{up}\|[001]$, $\mathbf{P}_{dn}\|[00\bar{1}]$) in the BTO supercells.

		1 ML Fe		2 ML Fe (FI)		3 ML Fe	
m_s [μ_B]		P_{up}	P_{dn}	P_{up}	P_{dn}	P_{up}	P_{dn}
S3	Fe					1.77	1.87
S2	Fe(Ti)			− 2.13	− 1.94	1.50	1.51
S2	Fe(Ba)			2.28	2.17	1.27	1.23
S1	Fe	2.83	2.84	0.0	0.0	1.09	1.00
I	Ti	− 0.21	− 0.07	0.0	− 0.01	− 0.09	− 0.01
I	O	0.09	0.10	0.0	0.0	0.02	0.02

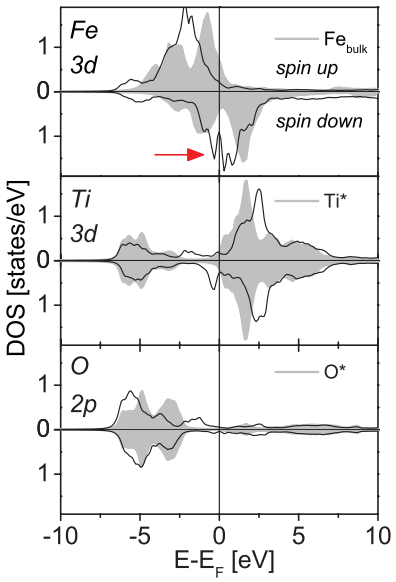

FIG. 2. (Color online) Calculated spin-resolved DOS of Fe 3d, Ti 3d, and O 2p states for 1 ML Fe/BTO and polarization $\mathbf{P}_{up}$ (solid lines). Ti* and O* denote bulklike states in the supercell (gray areas). Fe_{bulk} stands for a Fe-bcc bulk calculation.

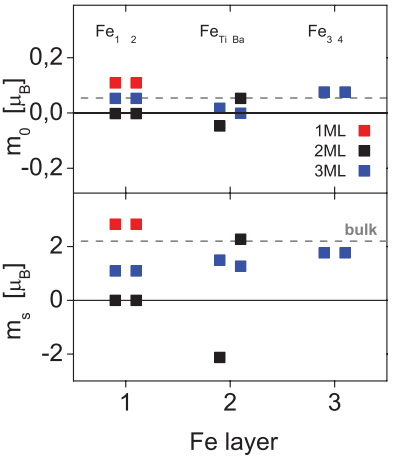

FIG. 3. (Color online) Calculated layer-resolved magnetic spin (m_s) and orbital (m_o) moments of Fe atoms in dependence on the thickness of Fe layers on BTO and polarization $\mathbf{P}_{up}$ (SPR-KKR method). Note that there are two atoms per unit cell in each layer.

the published values.[3] There are differences concerning the induced magnetic moments at the interface, which are however not in the focus of our XMCD discussion of Fe $L_{2,3}$ edges.

The magnetic properties of the system are a result of competition between the reduced coordination number of Fe atoms at the surface and interface and the relaxation of the system. The last one determines the strength of hybridization between Fe 3d and Ti 3d states on the one hand and Fe 3d and O 2p states on the other hand. This may give rise to an enhanced or decreased magnetic moments.[1–3]

Although a detailed discussion of electronic structure and magnetism is not in the focus of this work, we give a short summary of the main results concerning the Fe/BTO interface in the multilayer system $(Fe_2)_m/(BTO)_5$ ($m = 1,2,3$). For 1 ML of Fe a ferromagnetic ground state is obtained, where the magnetic moment of Fe atoms in the surface $S1$ is much larger as for Fe_{bulk} atoms. As shown in Fig. 2 the reduced coordination number at the surface (in comparison to Fe_{bulk} leads to d-band narrowing.[41] We get a much higher density of unoccupied spin-up d states and observe much more fine structures near the Fermi energy due to the lower symmetry and additional surface states in comparison to Fe_{bulk}. Besides, we observe an induced magnetic moment at the Ti and O atoms at the interface I, respectively. In Fig. 2 we compare the spin-resolved DOS of 3d states (2p states) of Ti (O) atoms at the interface to Ti* (O*) atoms of bulklike states. The induced magnetic moment of the Ti atoms is opposite to the direction of the magnetic moment of Fe atoms in the surface $S1$.

In case of 2 ML Fe a ferromagnetic as well as a ferrimagnetic state are found.[3] From total energy calculations it follows that the ferrimagnetic (FI) state is preferred in comparison to the ferromagnetic (FM) one. The difference $\Delta E_{tot} = |E_{tot}^{(FM)} - E_{tot}^{(FI)}|$ amounts to 0.02 meV.[2] In the FI state the magnetic moments of Fe_{Ba} and Fe_{Ti} in layer $S2$ are different and align in opposite directions (see Table II). The magnetic moment of Fe atoms in layer $S1$ is strongly suppressed in comparison to $S2$ and does not contribute essentially to the magnetic behavior of the system. Also the induced magnetic moments of Ti and O atoms at the interface are very small. In the 3 ML case again the ferromagnetic state is preferred. The magnetic moment of the Fe atoms in the surface $S3$ is smaller than for Fe bulk or the Fe surface $S1$ in the 1 ML case, respectively.

The dependence on the direction of polarization $\mathbf{P}$ (Table II) is caused mainly by the change of the distances between Fe and Ti (O) atoms at the interface, respectively. A larger (smaller) value means a smaller (larger) hybridization between the Fe and Ti 3d states (O 2p states) and therefore a larger (smaller) magnetic moment (see Table II). This dependence of the induced magnetic moments on the electric polarization reversal in BTO determines the interface magnetoelectric coupling.

We extended our calculations using a fully relativistic KKR method.[36] This places us in the position to calculate magnetic orbital moments of the multilayer system. With regards to the limitation of DFT-LDA (neglecting orbital corrections) we find general trends in dependence on the Fe layer thickness as shown in Fig. 3. As expected the quenching of the orbital moment is partly lifted in the 1 ML case in comparison to Fe_{bulk}.[41] In the 2 ML and 3 ML case the orbital moment is reduced in comparison to the 1 ML case and quenched as in the Fe(bcc) case, respectively.

B. X-ray absorption spectra and x-ray magnetic circular dichroism calculations

In our simulations of XAS and XMCD the magnetization $\mathbf{M}$, the electric polarization $\mathbf{P}$ and the incidence of light are parallel to the z axis (surface normal) of the Fe/BTO(001) system (see Fig. 1). All x-ray absorption spectra are broadened by Lorentz convolution with a core hole width of 0.4 eV and 0.2 eV for the L_2 and L_3 edge, respectively.

In Fig. 4 the calculated x-ray absorption spectra for right (–) and left (+) circularly polarized light (upper part) and the

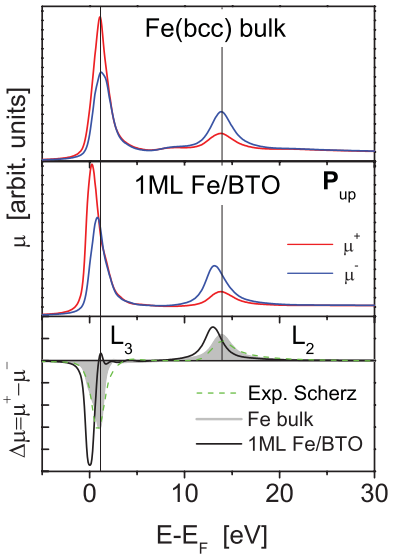

FIG. 4. (Color online) Calculated x-ray absorption spectra of Fe $L_{2,3}$ edges in Fe_{bulk} (upper part) and for 1 ML Fe/BTO(001) ($\mathbf{P}_{up}$). In the lower part the related difference spectra $\Delta\mu$ are shown. The calculated XMCD of Fe_{bulk} is shown in comparison to available experimental results taken from Scherz *et al.*[42] (dashed line).

related difference spectra $\Delta\mu$ (lower part) are shown for 1 ML Fe/BTO ($\mathbf{P}_{up}$) in comparison to calculations performed for Fe_{bulk}. The calculated XMCD of Fe_{bulk} is compared to available experimental results[42] to emphasize the quality of our SPR-KKR calculations.

In both cases we observe the well -known energy dependence of XMCD in a ferromagnetic system. Using right circularly polarized (–) light the intensity at the L_3 (L_2) edge is enhanced (decreased) due to different selection rules of spin-up and spin-down electrons in the ferromagnetic phase. The behavior is opposite at the L_3 (L_2) edge in case of left circularly polarized (+) light. Band structure effects determine the spectral shape of the XMCD.

In the 1 ML case the maximum of the L edges of left and right circularly polarized light is not at the same energetic position as observed for Fe_{bulk} (see vertical lines in Fig. 4). This is related to the l-projected DOS, where we have found a small split in the Fe DOS of d electrons (see red arrow in Fig. 2) just above the Fermi energy. The reason for this behavior lies in the cancellation of degenerate d states in systems of reduced symmetry and the appearance of surface states.

The results of XMCD for 1 ML, 2 ML, and 3 ML are summarized in Fig. 5. In the 2 ML case we have calculated the x-ray absorption spectra and the related differences $\Delta\mu$ for both the ferrimagnetic and the ferromagnetic state as shown in Fig. 5 (middle part). The XMCD of the ferrimagnetic phase is small and follows the well-known behavior of antiferromagnetic/ferrimagnetic states. In case of the ferromagnetic state we get a small fine structure in the energy dependence of the L_3 edge, which we find also in the 3 ML case (upper part), which is discussed in more detail in the following chapter. The dependence on the electric polarization $\mathbf{P}$ of BTO is in all cases very weak as indicated exemplary in the 3 ML case (dashed line in Fig. 5).

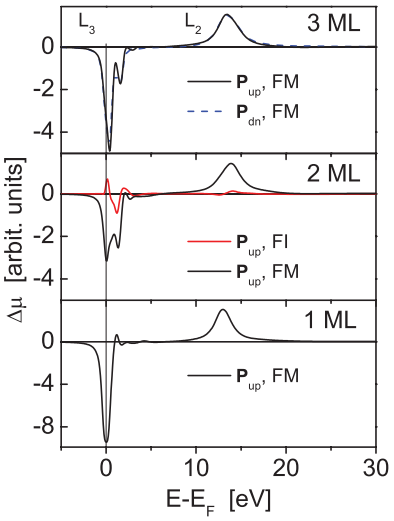

FIG. 5. (Color online) Calculated XMCD of the $L_{2,3}$ edge of Fe for 1 ML, 2 ML, and 3 ML Fe/BTO(001). The dependence on the polarization $\mathbf{P}$ is shown for the 3 ML case (dashed curve in the upper part). In case of 2 ML both the ferromagnetic (FM) and ferrimagnetic (FI) ground states are displayed.

C. Layer-resolved x-ray magnetic circular dichroism

The characteristic energy dependence of the L_3 edge (L_2 edge) is directly related to the reduced symmetry at the interface and surface Fe multilayer system, respectively. In our calculations we can separate the different contributions of the total XMCD. In Fig. 6 the layer-resolved XMCD of ferromagnetic 2 ML and 3 ML Fe/BTO(001) are shown normalized to the number of Fe atoms in the unit cell of the system. While both Fe atoms in layer $S1$ ($Fe_{1,2}$) and $S3$ ($Fe_{3,4}$) are equivalent, the Fe atoms in layer $S2$ are at nonequivalent positions (Fe_{Ba} and Fe_{Ti}), which leads to small differences in the XMCD signal. Besides we show the dependence on the direction of polarization for Fe atoms at the interface and surface (solid lines for $\mathbf{P}_{up}$ and dashed lines for $\mathbf{P}_{dn}$ in Fig. 6).

In the energy dependence of the L_3 edge we observe a splitting of the XMCD peak with respect to energy in

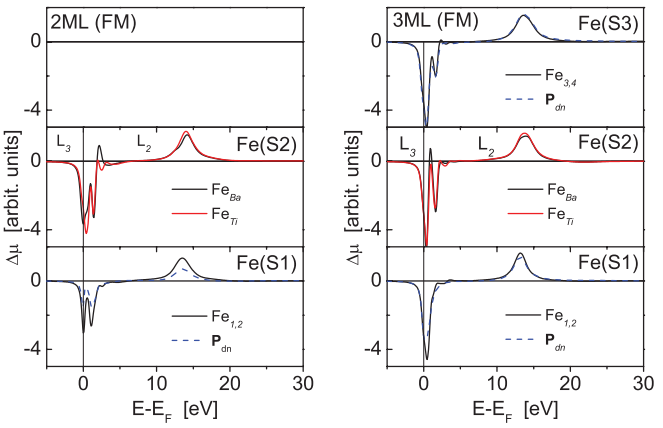

FIG. 6. (Color online) Layer-resolved XMCD of Fe $L_{2,3}$ edges of ferromagnetic 2 ML (left) and 3 ML (right) Fe on BTO ($\mathbf{P}_{up}$). The interface and surface $\mathbf{P}_{up}$ results are compared to $\mathbf{P}_{dn}$ data (dashed lines).

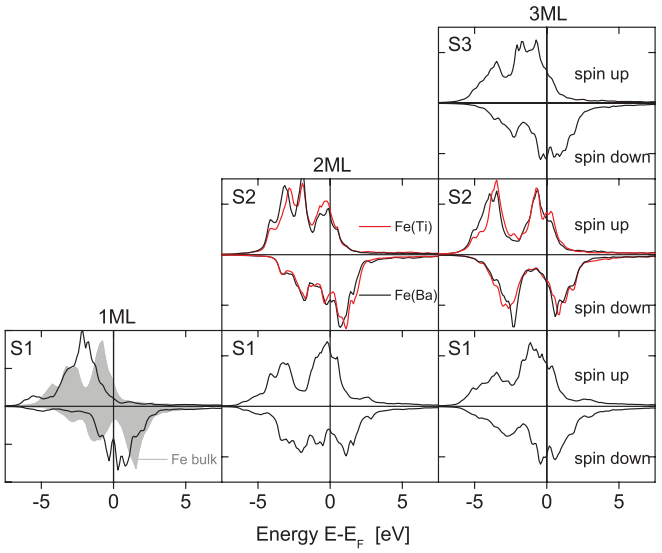

FIG. 7. (Color online) Layer- and spin-resolved DOS of Fe 3*d* states in Fe/BTO(001). Results are shown for $\mathbf{P}_{up}$ in dependence on the layer thickness (1 ML, 2 ML, and 3 ML). *S*1, *S*2, and *S*3 denotes the layer number starting from the TiO_2 interface *I* with *S*1. In the second Fe layer (2 ML and 3 ML case) we have two different Fe positions on Ti and Ba atoms, respectively. The gray area (see 1 ML, *S*1) is the calculated DOS of Fe 3*d* states in Fe_{bulk}.

dependence on the layer thickness. The appearance of this structure can be explained if we consider the spin- and layer-resolved DOS of the Fe *d* states as shown in Fig. 7. In comparison to Fe_{bulk} (gray area) we observe many more structures in the layer system. These structures depend strongly on the layer thickness and the position of the layer (surface, interface, or between both). The DOS at the Fermi level is very sensitive with regard to the relaxed structure at the interface or surface. We observe more and different states, for example due to hybridization, as in the bulk situation. To have a close look at the XMCD we apply a simple one-electron model.

In the one-electron picture the absorption coefficient $\mu^{\lambda,\sigma}(E)$ depends on the transition probability $M_L^{\lambda,\sigma}$ and the density of states $n_L^{\sigma}(E)$

$$\mu^{\lambda,\sigma}(E) \propto \sum_L M_L^{\lambda,\sigma}\, n_L^{\sigma}(E), \tag{2}$$

where λ and σ denote the kind of light and electron spin polarization, respectively. The quantity $L = (l,m)$ stands for the quantum numbers of the angular momentum operator. The transition probability $M_L^{\lambda,\sigma}$ is a smooth function of energy, which we neglect in the following discussion for simplicity. The selection rules of L in dependence on the polarization of light are well known and documented.[43]

In case of spherical symmetry the density of states $n_L^{\sigma}(E)$ does not depend on the m values for a given angular momentum l. Assuming that the spin-up channel is completely occupied the XMCD $\Delta\mu$ of the L_3 edge ($p_{3/2}$) is determined by the sum of all spin-down contributions. We find: $\Delta\mu(L_3) \propto [-10\, n_d^{\downarrow}]$. For the cubic case we obtain for $l = 2$ an energy splitting between the states with $m = 0,2$ (forming the e_g states) and $m = -2, -1,1$ (forming the t_{2g} states). This gives us the contribution $\Delta\mu(L_3) \propto [8\, n_{e_g}^{\downarrow} - 18\, n_{t_{2g}}^{\downarrow}]$, which determines the main contribution of the XMCD signal of the L_3 edge for cubic symmetry. At the surface or interface the degeneration between $m = 0$ and $m = 2$ and between $m = -1,1$ and $m = -2$ is suppressed, respectively. Therefore, we observe more structures in the XMCD of the Fe multilayer system in comparison to a bulklike system (Fig. 4). In general it is possible to separate all the different contributions in layer-resolved XMCD calculations. This dependence on layer thickness should show up in corresponding experiments.

TABLE III. Calculated critical temperatures of the Fe/BTO system in dependence on the Fe-layer thickness for two values of the MAE parameter and different magnetic phases.

T_c [*K*]	1 ML	2 ML		3 ML
MAE [meV]	FM	FM	FI	noncollinear
0.5	190	222	88	170 ($\pm$10)
1.0	204	230	85	170 ($\pm$10)

D. Calculation of critical temperature

Heisenberg exchange parameters J_{ij} follow directly from the KKR Green's function by means of the magnetic force theorem.[37] The exchange parameters are calculated for the different layer thicknesses and magnetic structures. Classical Heisenberg Hamiltonians in Monte Carlo (MC) simulations are used to determine the critical temperatures. For importance sampling the Metropolis algorithm is applied. The critical temperatures are extracted from the fourth-order cumulant.[38] More details can be found in Ref. 39. The magnetocrystalline anisotropy energy (MAE) is considered as a parameter and set to reasonable values in the MC simulations. In case of Fe_{bulk} we get $T_c = 950 \pm 10$ K. This is in reasonable agreement with the experimental value of 1043 K and as well to other previous *ab initio* estimates obtained with MC simulations.[44,45] The fact, that our values are lower can be explained by the differences in the obtained J_{ij} and by the larger number of interaction shells taken for the MC simulations in our work (17 compared to 2 and 1). In Table III the results of our calculations are summarized for the considered Fe/BTO(001) system. In all cases the critical temperature is clearly below room temperature. This result is independent on the MAE parameter chosen in the simulation. We will expand these investigations to obtain further insight into the nature of long-range magnetic interaction.

IV. CONCLUSION

We employ first-principles calculations to study x-ray absorption spectra and XMCD of the multiferroic system Fe/BTO(001). Our main goal was to study both the influence of structural and magnetic properties of the Fe films and the dependence on the polarization direction of BTO. Our calculations show that x-ray absorption spectroscopy and XMCD measurements are essential to understand the complex magnetic behavior at the interface and surface of this system. The differences in the magnetic properties in dependence on the layer thickness are directly reflected in the behavior of x-ray

absorption spectra of the Fe $L_{2,3}$ edges and the related XMCD. We have found however only a very weak dependence on the polarization direction **P** of BTO. Nevertheless, the XMCD in the monolayer thickness region can form a bridge across first-principles calculations and experiments of multiferroic systems.

The starting point of the spectroscopic calculations in the framework of a fully relativistic method was the fully relaxed structure of the system, which was imported from a pseudopotential calculation. Our calculated magnetic spin and orbital moments of the Fe atoms depend strongly on the local structure of the Fe multilayers, where we may separate the influence of surface and interface effects for Fe/BTO(001). The quenched orbital moment of Fe-bcc bulk is partly lifted in dependence on the Fe layer thickness. The magnitude of the local magnetic moments depends on the details of the DOS mainly determined by the behavior of the Fe *d* electrons.

The XMCD of the Fe layers (1–3 ML) on a TiO_2-terminated BTO(001) surface shows characteristic structures, which are related to the changes of the structure at the Fe/BTO interface or Fe surface. This gives rise to a rich fine structure in the DOS of the Fe *d* states near the Fermi energy.

Our results show that XMCD experiments will fail at room temperature because of the low critical temperature of the Fe films. Experiments at low temperature might give interesting insight into the structural, electronic, and magnetic properties of this system.

ACKNOWLEDGMENTS

We are grateful for financial support by Deutsche Forschungsgemeinschaft in the framework of SFB762 Functionality of Oxide Interfaces. The authors would like to thank Hubert Ebert's group (Munich) for the introduction to the SPR-KKR program and helpful discussions.

[1] C. G. Duan, R. F. Sabirianov, W. N. Mei, S. S. Jaswal, and E. Y. Tsymbal, Nano Letters **6**, 483 (2006).
[2] M. Fechner, S. Ostanin, and I. Mertig, Phys. Rev. B **77**, 094112 (2008).
[3] M. Fechner, I. V. Maznichenko, S. Ostanin, A. Ernst, J. Henk, P. Bruno, and I. Mertig, Phys. Rev. B **78**, 212406 (2008).
[4] T. Cai, S. Ju, J. Lee, N. Sai, A. A. Demkov, Q. Niu, Z. Li, J. Shi, and E. Wang, Phys. Rev. B **80**, 140415(R) (2009)
[5] S. Valencia, A. Crassous, L. Bocher, V. Garcia, X. Moya, R. O. Cherifi, C. Deranlot, K. Bouzehouane, S. Fusil, A. Zobelli, A. Gloter, N. D. Matur, A. Gaupp, R. Abrudan, F. Radu, A. Barthéély, and M. Bibes, Nature Mater. **10**, 753 (2011).
[6] G. Schütz, W. Wagner, W. Wilhelm, P. Kienle, R. Zeller, R. Frahm, and G. Materlik, Phys. Rev. Lett. **58**, 737 (1987).
[7] C. T. Chen, F. Sette, Y. Ma, and S. Modesti, Phys. Rev. B **42**, 7262 (1990).
[8] C. Vaz, J. Bland, and G. Lauhoff, Rep. Prog. Phys. **71**, 056501 (2008).
[9] M. Finazzi, D. Lamberto, and F. Ciccacci, Surf. Sci. Rep. **64**, 139 (2009).
[10] D. Spisak and J. Hafner, Phys. Rev. B **73**, 155428 (2006).
[11] V. Cros, F. Petroff, J. Vogel, A. Fontaine, J. L. Menendez, A. Cebollada, W. Grange, J. P. Kappler, M. Finazzi, and N. Brookes, Europhys. Lett. **49**, 807 (2000).
[12] H. L. Meyerheim, J. M. Tonnerre, L. Sandratskii, H. C. N. Tolentino, M. Przybylski, Y. Gabi, F. Yildiz, X. L. Fu, E. Bontempi, S. Grenier, and J. Kirschner, Phys. Rev. Lett. **103**, 267202 (2009).
[13] H. L. Meyerheim, R. Popescu, J. Kirschner, N. Jedrecy, M. Sauvage-Simkin, B. Heinrich, and R. Pinchaux, Phys. Rev. Lett. **87**, 076102 (2001).
[14] H. L. Meyerheim, R. Popescu, N. Jedrecy, M. Vedpathak, M. Sauvage-Simkin, R. Pinchaux, B. Heinrich, and J. Kirschner, Phys. Rev. B **65**, 144433 (2002).
[15] C. Tusche, H. L. Meyerheim, N. Jedrecy, G. Renaud, and J. Kirschner, Phys. Rev. B **74**, 195422 (2006).
[16] P. Torelli, S. Benedetti, P. Luches, L. Gragnaniello, J. Fujii, and S. Valeri, Phys. Rev. B **79**, 035408 (2009).
[17] P. Luches, M. Liberati, and S. Valeri, Surf. Sci. **532-535**, 409 (2003).
[18] A. D. Alvarenga, F. Garcia, L. C. Sampaio, C. Giles, F. Yokaichiya, C. A. Achete, R. A. Simao, and A. P. Guimaraes, J. Magn. Magn. Mater. **233**, 74 (2001).
[19] S. Brivio, D. Petti, R. Bertacco, and J. C. Cezar, Appl. Phys. Lett. **98**, 092505 (2011).
[20] S. Brivio, C. Rinaldi, D. Petti, R. Bertacco, and F. Sanchez, Thin Solid Films **519**, 5804 (2011).
[21] S. Sahoo, S. Polisetty, Chun-Gang Duan, S. S. Jaswal, E. Y. Tsymbal, and C. Binek, Phys. Rev. B **76**, 092108 (2007).
[22] C. Yu, M. J. Pechan, S. Srivastava, C. J. Palmstrøm, M. Biegalski, C. Brooks, and D. Schlom, J. Appl. Phys. **103**, 07B108 (2008).
[23] V. Garcia *et al*., Science **372**, 1106 (2010)
[24] H. L. Meyerheim, F. Klimenta, A. Ernst, K. Mohseni, S. Ostanin, M. Fechner, S. Parihar, I. V. Maznichenko, I. Mertig, and J. Kirschner, Phys. Rev. Lett. **106**, 087203 (2011).
[25] The structure is visualized using VESTA: a three-dimensional visualization system for electronic and structural analysis, K. Momma and F. Izumi, J. Appl. Crystallogr. **41**, 653 (2008).
[26] G. Kresse and J. Furthmüller, Phys. Rev. B **54**, 11169 (1996); G. Kresse and D. Joubert, *ibid*. **59**, 1758 (1999).
[27] Jürgen Hafner, J. Comput. Chem. **29**, 2044 (2008).
[28] H. Ebert, Rep. Prog. Phys. **59**, 1665 (1996).
[29] J. Korringa, Physica **13**, 392 (1947); W. Kohn and N. Rostoker, Phys. Rev. **94**, 1111 (1954).
[30] P. Weinberger, *Electron Scattering Theory of Ordered and Disordered Matter* (Oxford University Press, Oxford, 1990), and references therein.
[31] P. Strange, *Relativistic Quantum Mechanics* (Cambridge University Press, Cambridge, 1998), and references therein.
[32] M. Lüders, A. Ernst, W. M. Temmerman, Z. Szotek, and P. J. Durham, J. Phys.: Condens. Matter **13**, 8587 (2001).
[33] G. Y. Guo, Phys. Rev. B **57**, 10295 (1998).
[34] Chemical Analysis, Vol. 92, *X-ray Absorption: Principles, Applications and Techniques of EXAFS, SEXAFS and XANES*, edited by D. C. Koningsberger and R. Prins, (Wiley, New York, 1976).

[35]J. Stöhr, H. A. Padmore, S. Anders, T. Stammler, and M. R. Scheinfein, Surf. Rev. Lett. **5**, 1297 (1998).
[36]H. Ebert *et al*., The Munich SPR-KKR package, version 5.4 [http://olymp.cup.uni-muenchen.de/ak/ebert/SPRKKR]; H. Ebert, in *Electronic Structure and Physical Properties of Solids*, edited by H. Dreyssé, Lecture Notes in Physics, Vol. 535 (Springer, Berlin, 1999), p. 191.
[37]A. I. Liechtenstein, M. I. Katsnelson, V. P. Antropov, and V. A. Gubanov, J. Magn. Magn. Mater. **67**, 65 (1987).
[38]K. Binder, Z. Phys. B **43**, 119 (1981).
[39]G. Fischer, M. Däne, A. Ernst, P. Bruno, M. Lueders, Z. Szotek, W. Temmerman, and W. Hergert, Phys. Rev. B **80**, 014408 (2009).
[40]H. J. Monkhorst and J. D. Pack, Phys. Rev. B **13**, 5188 (1976).
[41]R. Skomski, *Simple Models of Magnetism* (Oxford University Press, Oxford, 2008).
[42]A. Scherz, H. Wende, and K. Baberschke, Appl. Phys. A **78**, 843 (2004)
[43]G. van der Laan, J. Magn. Magn. Mater. **156**, 99 (1996).
[44]J.-T. Wang, L. Zhou, D.-S. Wang, and Y. Kawazoe, Phys. Rev. B **62**, 3354 (2000).
[45]N. M. Rosengaard and B. Johansson, Phys. Rev. B **55**, 14975 (1997).